Resting Myosin Cross-bridge Configuration in Frog Muscle Thick Filaments

Marie Cantino* and John Squire‡

*Center for Bioengineering, University of Washington, Seattle, Washington 98195; and ‡Biophysics Section, Blackett Laboratory, Imperial College, London SW7, England

Abstract. Clear images of myosin filaments have been seen in shadowed freeze-fracture replicas of single fibers of relaxed frog semitendinosus muscles rapidly frozen using a dual propane jet freezing device. These images have been analyzed by optical diffraction and computer averaging and have been modelled to reveal details of the myosin head configuration on the right-handed, three-stranded helix of cross-bridges. Both the characteristic 430-Å and 140–150-Å repeats of the myosin cross-bridge array could be seen. The measured filament backbone diameter was 140–160 Å, and the outer diameter of the cross-bridge array was 300 Å. Evidence is presented that suggests that the observed images are consistent with a model in which both of the heads of one myosin molecule tilt in the same direction at an angle of ~50–70° to the normal to the filament long axis and are slewed so that they lie alongside each other and their radially projected density lies along the three right-handed helical tracks. Any perturbation of the myosin heads away from their ideal lattice sites needed to account for x-ray reflections not predicted for a perfect helix must be essentially along the three helical tracks of cross-bridges. Little trace of the presence of non-myosin proteins could be seen.

A thorough knowledge of the structure of the myosin-containing filaments in both muscle and non-muscle contractile systems is clearly essential if the mechanism of force production in these systems is to be understood. In particular, x-ray diffraction analysis of cross-bridge movements associated with contraction (9, 10) is likely to require the prior knowledge of the cross-bridge organization on the myosin filaments in relaxed muscle (24).

The last few years have seen a significant advance in myosin filament studies. Beautiful electron micrographs of isolated myosin filaments from various invertebrate muscles have now been obtained (14, 19, 30) and these show for the first time excellent preservation of the helical arrays of myosin cross-bridges. In all cases, details of the organization of cross-bridges within the helical arrays have been obtained by optical diffraction and by three-dimensional reconstruction methods. More recently, electron micrographs of much improved preparations of isolated vertebrate muscle myosin filaments have been obtained (13). These confirm the three-stranded helical symmetry of the myosin cross-bridge array (23), and they show that the strands are right-handed. However, apart from the general conclusion that the cross-bridge density lies essentially along these strands, there appears to be little detailed information so far about the organization of myosin heads within the three-stranded helix.

Another approach to the study of myosin filament structure is to optimize the preservation of the cross-bridge array in whole muscle fibers by means of rapid freezing methods (1, 2, 7). The ultrastructure in the fibers can then be visualized using freeze-fracturing, deep-etching, heavy metal shadowing, and carbon replication. As was reported in early 1983 by Cantino and Pollack (1), such an approach to the study of mechanically skinned fibers from frog semitendinosus muscles, in this case frozen by a propane jet freezing device (17), does indeed preserve the helical array of cross-bridges. The replicas show the expected repeats of 430 and 143 Å, both of which are characteristic of vertebrate muscle thick filaments. Recently two reports of analogous studies of relaxed rabbit muscle frozen on a helium-cooled copper block (slammer) device have been published. Although in the first (11) little helical structure was seen, the second (12) showed micrographs with improved preservation of the three right-handed helical tracks of cross-bridges. However there was little indication of the characteristic 143-Å cross-bridge repeat. We have now carried out image analysis and modelling studies of a selection of the frog muscle replicas obtained using the propane jet freezing method. We have found not only that they confirm the three-stranded symmetry of the cross-bridge helix and its right-handedness, but also that they show clearly the 143-Å cross-bridge repeat and provide information about the configuration of the myosin heads within this repeat.

Materials and Methods

Freeze-Fracture Replicas

Myosin filaments used in this study were from samples frozen in a dual propane jet freezing device (2). Single fibers from the semitendinosus muscle of frogs

(*R. temporaria*) were removed from the muscle, mechanically skinned, and mounted between two hooks in a relaxing solution containing 110 mM KCl, 3 mM $MgCl_2$, 2.5 mM ATP, 5 mM EGTA, and 10 mM Imidazole, at 10°C, adjusted to pH 7.0. Rapidly frozen samples were fractured at −105 to −110°C in a Balzers BAF 301 freeze-fracture unit (Balzers, Hudson, NH), etched for 4 min at −95°C, and unidirectionally shadowed with ~30 Å of Pt-C. Replicas were cleaned in bleach, picked up on formvar-coated grids, and viewed in an electron microscope (JEOL USA, Peabody, MA). For a description of the freeze-fracture, deep-etch technique see Heuser (7).

Optical Diffraction

Optical diffraction patterns were recorded from contrasty copies of the original micrographs using a horizontal laser diffractometer of conventional design (15). Negatives were immersed in oil, when necessary, to reduce phase artifacts due to variations in emulsion thickness.

Image Processing

Translationally averaged images of selected filaments were produced by processing the appropriate areas of 256 × 256 pixel images with 256 grey levels obtained using a Microsight T.V. imaging system (Digithurst Ltd., Royston, Cambridge, England) and a SIRIUS microcomputer. Magnifications of the originals were chosen to give ~30–40 pixels per 430-Å repeat, corresponding to a pixel resolution of ~10–15 Å. Average images were displayed on the computer screen and either photographed directly or dumped to a dot matrix printer. Alternatively, average images were printed out as number arrays for contouring.

Results

Appearance of the Cross-bridge Helix

Images of myosin filaments in single skinned fiber preparations were obtained from 10 frogs. Although the degree of helical order varied from sample to sample, a majority of fibers frozen under relaxing conditions contained many filaments where a myosin helix was readily discernable. A good example is shown in Fig. 1. In all cases the angle subtended between the source and the plane of the fracture surface (horizontal) was 40°. Within this plane the projected direction of shadowing could be varied through an angle (θ) between 0° and 90° relative to the long axis of the muscle fibers. To reveal different aspects of the cross-bridge arrays, several different shadowing angles (θ) were used. In some cases, where the filament lattice was disrupted, filaments at several angles were found within the same sample. However, here too the shadowing angle for each filament could still be determined. All of the filaments discussed here were shadowed at an angle (θ) of ~20°. This particular shadowing angle gave images in which both the 430 Å and 140–150-Å repeats were clearly delineated. Results from filaments shadowed at different angles will be presented elsewhere. We selected the most highly ordered regions for our analysis, and some typical examples are presented in Fig. 2. Filaments were characterized by helical turns similar to those reported by Ip and Heuser (12), with a measured axial spacing of 390–430 Å, presumed to be the known 430-Å helical repeat of myosin. In addition, helical gyres were punctuated by clear subunits with an axial spacing of approximately one-third of the helical repeat. This was presumed to correspond to the characteristic 143-Å myosin repeat. The hand of the helix could be determined directly from samples in which we were careful to keep the replica upright during cleaning, and was confirmed to be right-handed by comparison with the right-handed, long-period strands of the actin helix visible in parts of some sarcomeres.

Optical Diffraction

Images of single myosin filaments were analyzed both by optical diffraction and by real space image averaging methods. Fig. 2, *e* and *f* are typical examples of the optical diffraction patterns from these filaments. Clearly visible is a series of layer lines that can be indexed on the measured thick filament repeat of ~400 Å. By analogy with x-ray diffraction patterns from intact vertebrate skeletal muscles, the first layer line (l = 1), with its strong off-meridional component, was taken to correspond to the 430-Å x-ray layer line (8). Similarly, the third-order reflection, usually with greatest intensity on or close to the meridian, was taken to correspond to the 143-Å meridional x-ray reflection (l = 3).

The appearance of these diffraction patterns is generally consistent with the expected transform of a one-sided helical structure with the known thick filament helical symmetry. However, some interesting features were also seen. For example, meridional intensity was often seen on the first, second, fourth, and fifth layer lines, with the first, second, and fifth meridional reflections being the strongest and the most frequent. Such intensity, which is also seen in x-ray diffraction patterns from relaxed frog muscle (5, 8), would not be expected from a simple helix. It has previously been accounted for largely in terms of a perturbation of the cross-bridge axial repeat from a regular 143-Å spacing (20, 24, 27, 32). Cross-bridge intervals of ~160 Å, 120 Å, and 140 Å have been observed in cryo-sections of human muscle (27), and diffraction patterns of micrographs of this and other higher vertebrate muscles have often shown strong second- and fifth-order meridional reflections.

In the case of the shadowed filaments described here, there is an added complication in the analysis of axial perturbations. Some of the observed features may be due to the fact that even perfectly helical arrays of subunits shadowed unidirectionally would not be expected to appear as perfect one-sided helices. This is because the repeating subunits on the helix will be at different azimuths around the helix axis relative to the heavy metal source and will thus be shadowed in slightly different ways. This means that the shadowed frog muscle myosin filaments shown here, although appearing approximately helical, will actually have a periodic pattern of shadowing on them with a true repeat of 430 Å; slightly non-equivalent shadowing of myosin would occur on myosin heads separated axially by either 143 Å or 2 × 143Å. This could, in principle, lead artificially to the generation of forbidden meridional reflections, for example, on the first, second, fourth, and fifth layer lines. However, the fact that the strongest meridional reflections in our patterns do correspond to those seen in x-ray diffraction patterns suggests that such effects may be relatively minor compared with the known cross-bridge perturbations. The nature of the axial perturbations seen in these filament replicas will be discussed elsewhere.

Image Averaging

In order to see more details of the density features spaced at 140–150-Å intervals, we have carried out averaging of the filament images by translations along the filament axis equal to the axial repeat of 430 Å. Because of the possible non-equivalence of the shadowing of successive subunits along the helix, and because of the intrinsic perturbations that may be present, it is not appropriate here to carry out helical averaging of the type that is conventionally used for images of negatively stained helical structures (3).

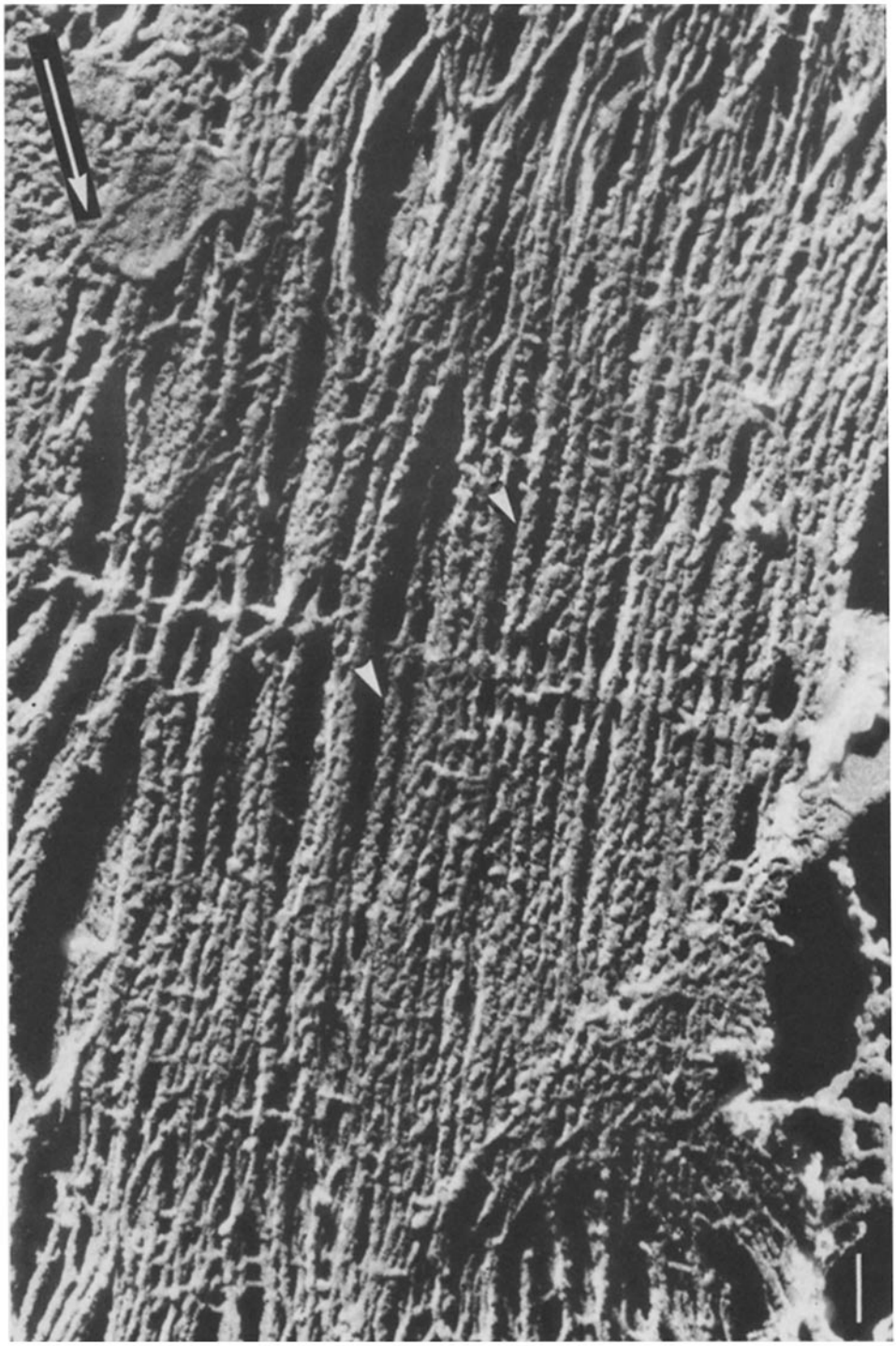

Figure 1. Image of a portion of a shadowed, deep-etched replica from a frog semitendinosus fiber. Electron microscope images here and in Fig. 2 have been photographically reversed so that the platinum appears white and shadows appear black. Large arrow indicates the direction of shadowing (angle θ), which was close to 20° to the fiber axis (see text). White arrowheads indicate filaments with particularly clear helical structures; they are included in Fig. 2. Bar, ~1,000 Å.

As described in Materials and Methods, filament images were processed using 256 × 256 pixel digital density arrays of each area of interest. Selected areas of each image were translationally averaged using between three and seven helical repeats. A number of such average images are shown in Fig. 3. Although many filaments within each sarcomere showed similar structures, we were careful to choose, where possible, those filaments that were well separated from their neighbors and showed clear edges. They have been arrayed in Fig. 3 with their repeats in approximate axial register so that their similarities are emphasized. It can be seen that all of the filaments show long clear helical strands of density along which are well-defined density peaks of spacing about one-third of the helix repeat. Slight variations in appearance occur in these and other averages in that some filaments show very deep diagonal shadows along the grooves between the helical strands, whereas others have more weakly contrasted grooves. This could be associated with slight variations either in the shadowing angle or in the depth of the filament in the fracture surface.

The outer diameter of the cross-bridge array (~300 Å) together with the backbone diameter, where it can be seen, of 140–160 Å, and the 430-Å axial repeat of these images, are all consistent with a three-stranded thick filament cross-bridge

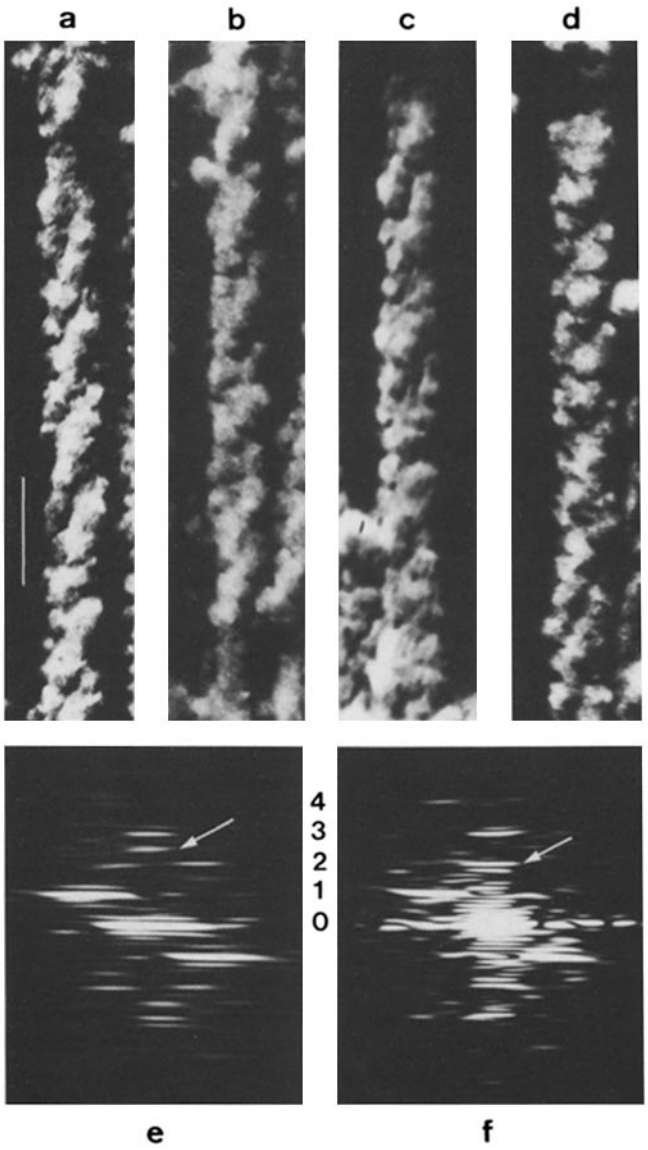

Figure 2. (*a–d*) Individual filaments from preparations as in Fig. 1 showing clear right-handed helical tracks of 140–150 Å-spaced subunits (bar, ~430 Å). *a* and *b* are from opposite sides of the M-band in the sarcomere in Fig. 1. Because of the dihedral symmetry of the thick filaments, the cross-bridge arrays therefore have opposite polarity in *a* and *b* and are thus shadowed in opposite directions. *e* and *f* are optical diffraction patterns from *a* and *d*, respectively (fiber axis vertical). They show clear layer lines at orders of 430 Å (labeled *1*, *2*, *3*, and *4*), but additional intensity is seen (arrowed) on the meridian in *f* at a spacing of ~215 Å (second layer line). In *e*, an additional reflection (arrowed) of spacing ~190 Å is unexplained.

helix with the center of mass of the cross-bridges at a radius of ~100–150 Å from the helix axis. These values for the backbone and outer diameters and the radius of the center of mass agree well with previous estimates (6, 12, 13, 24). From x-ray diffraction data (8) and using the point mass approximation with a J_3 Bessel function (24), the calculated center of mass would be at a radius of 134 Å.

Images such as those in Fig. 3, where the subunit position can be seen clearly, have these subunits disposed in relative positions very close to those expected for a perfect three-stranded 9/1 helix, as shown below using model structures. Note, however, that this must mean that any real perturbation of the cross-bridges away from the line of the helical tracks must be rather small; the perturbation must be essentially along the three long-pitched helical tracks. There is also a tendency for the density peaks on the 143-Å repeat to have elongated profiles that lie along these three tracks. Little evidence is seen of the presence of bulky extra proteins such as C-protein, X-protein, or H-protein (28). These may be closely associated with the filament backbone and may themselves be aligned along the long period helical tracks.

Analysis of the Myosin Head Configuration

Generation of Models

The images and optical diffraction patterns that we have obtained convincingly confirm the general structure predicted for the vertebrate myosin filament by x-ray diffraction and other techniques (i.e., three-stranded, with pitch and subunit axial repeats of 430 and 143 Å; reference 23). In principle they must also contain information about the configuration of the myosin cross-bridges on the thick filament surface. To understand better the images that might be produced by the unidirectional deposition of platinum-carbon on the cross-bridge array and to see if the technique has the potential to distinguish different cross-bridge configurations, we constructed several models with the symmetry and relative dimensions of vertebrate myosin filaments. In these models the heads could be arranged in any desired configuration. In an attempt to simulate the effects of the shadowing, we illuminated the (white) models against a black background using a point (projector) light source shining in the appropriate direction (θ = 20°). We also defocused the camera slightly to simulate the increased diameter and loss of resolution associated with the heavy metal layer. The individual heads could be oriented at any slew (α) and tilt (β) as defined in Fig. 4. The backbone radius (R in Fig. 4) and hence the inner end of the heads was set at ~75 Å.

Five of the models tested with this procedure are shown in Fig. 5. Fig. 5, *a–e* shows the appearance of each of the models with the α and β values indicated in the legend. The first two filaments (*a* and *b*) are based on x-ray diffraction modelling of the cross-bridge array in relaxed frog muscle by Haselgrove (6). The second pair of models (*c* and *d*) provides the current next best and best fits for the new x-ray diffraction data from relaxed fish (plaice fin) muscle (4). Of these, model *d* is very much preferred. The last model (*e*) is a modified version of *d* in which the heads are more closely associated with the filament backbone; they have a much larger tilt angle. Together, these models approximate to all of the classes of cross-bridge configuration that are consistent with the need to keep the cross-bridge density concentrated largely along the three long-pitched helices. Models *a*, *b*, and *e* have the centers of mass of the cross-bridges at radii of 130–140 Å as suggested by x-ray diffraction data. Models *c* and *d* have slightly larger radii.

The effects of two other variables were also modelled using this system. Photographs were taken of heads tilting both away from the light source (Fig. 6, top row) and towards the source (Fig. 6, bottom row). In addition, the models were photographed at two orientations differing by a rotation around the filament axis of 20°; a further rotation of 20°

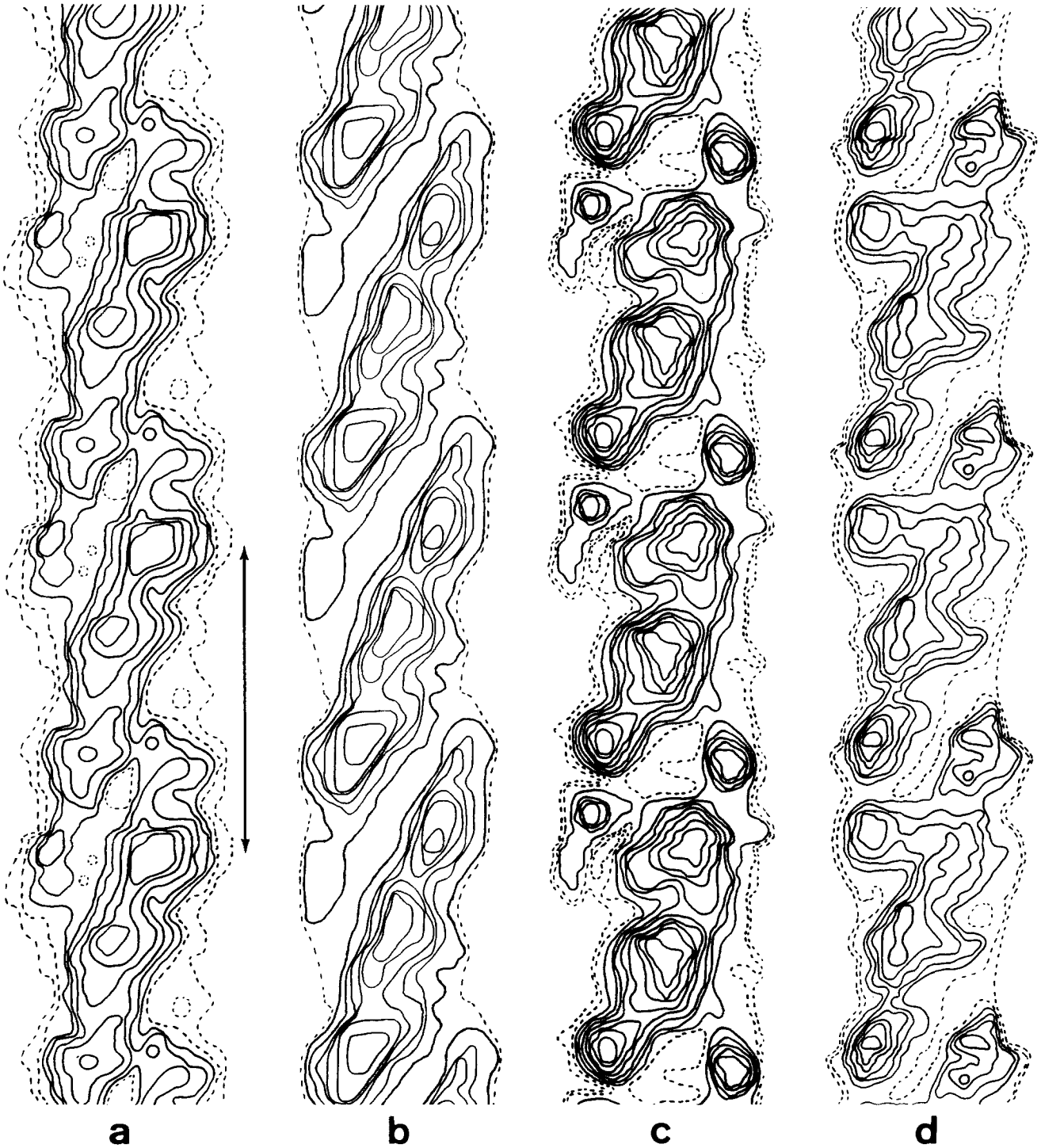

Figure 3. Translationally averaged images of individual filaments such as those in Fig. 2. Averages included (*a*) four repeats, (*b*) five repeats, (*c*) four repeats, and (*d*) three repeats. Density contour levels from ~30% to above 90% of maximum are shown. The lowest two levels are dotted. Most filaments have rather regular helical tracks of density peaks. These peaks tend to be elongated along the helical tracks so that the clefts between the helical tracks are well defined. The arrowed line shows the 430-Å repeat.

would return the models to their original configuration because of the 40° azimuthal separation of cross-bridges on the three-stranded 9/1 helix. However, it was found that the two azimuthal orientations of a particular model showed only minor differences in each case. For this reason we have shown only one orientation of each model in Fig. 6; only the effects of shadowing each structure from opposite ends are illustrated.

Comparison of Averages and Models

There is always a problem in trying to interpret electron micrographs of processed biological material in that some preparative artifacts are bound to occur and, to some extent, these may be unknown and variable in effect. However, in the present case, although (*a*) some disorder in the myosin

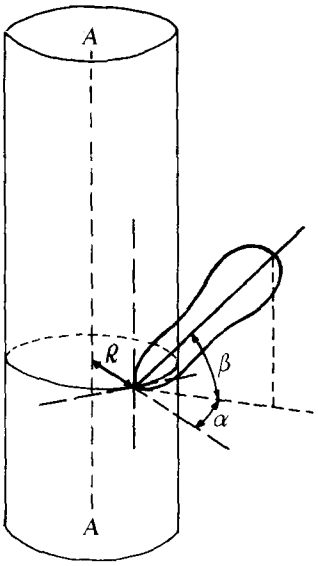

Figure 4. Definition of the slew angle (α) and tilt angle (β) used to describe myosin head orientation on the thick filament (axis vertical, *A-A*). Only one head of each pair is shown. *R* is the radius from the axis of the filament backbone to the inner ends of the myosin heads.

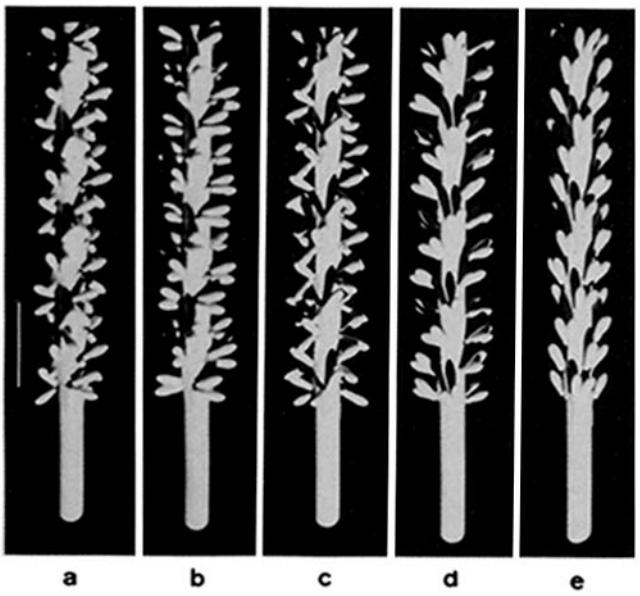

Figure 5. (*a–e*) Models with pairs of myosin heads arranged in a variety of configurations on the backbone surface of a three-stranded thick filament. Individual heads were modelled to be 160-Å long by ~50–55 Å in diameter (at the widest point). Head shape approximated to that used in Offer et al. (18). The backbone diameter was scaled to 150 Å. Pairs of heads were located precisely on the appropriately scaled lattice defined by a three-start helix with 430-Å pitch (bar) and 143-Å subunit axial repeat. No attempt was made to model a perturbation in the array. Models were constructed by fixing rubber policemen (pipette bulbs) to a metal post via pipecleaners, thus providing flexible joints between the heads and the backbone. Models were sprayed with a matt white paint to produce a uniform reflecting surface. Head positions in the five models were as follows: (*a*) α = +90°, +90°; β = +30°, −30°; (*b*) α = +60°, +60°; β = +20°, −20°; (*c*) α = +30°, +30°; β = +30°, −30°; (*d*) α = 0–+15°, +15–30°; β = +20–30°, +20–30°; (*e*) α = 0–+10°, +20–30°; β = +50–70°, +50–70°.

head array is inevitable, (*b*) some variation in the shadowing is likely to occur, and (*c*) the processing, including the effects of heavy metal deposition, may modify the structure slightly, the similarity of the observed structure to that predicted from x-ray diffraction data (see later comments) shows that detailed analysis of these images is both worthwhile and relevant to native relaxed thick filament structure. The use of average images will in any case reduce the effects of variable preservation and shadowing in successive repeats of the cross-bridge array.

In analyzing the different model images in Fig. 6 and comparing them with the observed average images shown in Fig. 3, a number of different factors can be taken into account. These are: (*i*) The apparent pitch angle of the helical tracks; a parameter related not only to the pitch length and the outer radius of the cross-bridges in the original models (Fig. 5), but also to the way in which the shadows in Fig. 6 highlight different features. The mean pitch angle in the averages in Fig. 3, as estimated from the slopes of lines visually fitted to the centers of the density peaks along the helical segments, is ~68° (±2°). Pitch angles similarly measured in Fig. 6 are about (*a*) 66°, (*b*) 60–65°, (*c*) 64°, (*d*) 65°, and (*e*) 69°. In each case (except *b*) these angles are probably accurate to within 2°. (*ii*) The general appearance of the shadowing along the three helical tracks giving the 430-Å repeat. Under the shadowing conditions that were used (i.e., θ = 20°) these tracks are clearly delineated as long, narrow, almost linear segments about five subunits (5 × 140–150-Å repeats) long. (*iii*) The similarity or differences between the same model illuminated from opposite ends. The observed filament images, although not identical, were not radically different on opposite sides of the M-band in a given sarcomere, as can be seen clearly in Fig. 1 (arrowed filaments) and Fig. 2, *a* and *b*. This rather surprising observation in view of the dihedral 32-point group symmetry of the vertebrate thick filament (16) is a strong constraint on possible models. Although our method of image defocusing will obviously not simulate exactly the effects of shadow thickness, these results do illustrate nevertheless the potential difficulty there could be, in models such as Fig. 5, *d* and *e* in which both heads tilt in the same direction, in defining whether this tilt is towards or away from the M-band.

On the basis of the various criteria listed above, we have concluded that on face value model *e* in Figs. 5 and 6 gives the most satisfactory results. In the images of models *b–d* in Fig. 6, the apparent pitch angle of the tracks of cross-bridges is ~60–65°, significantly less than the 68° in the average images in Fig. 3. Model *a* gives slightly better agreement (66°), but the slopes in the average images and in model *e* are rather close (68° and 69°). Secondly, models *b–d* do not show the strong delineation of the helical tracks observed in the average images in Fig. 3. These helical tracks are, however, clear in Fig. 6*e* and in Fig. 6*a*, top. Finally there are very obvious differences between models *a–d* when illuminated in opposite directions, whereas the observation is that only relatively subtle differences can be seen between filaments on opposite sides of a single M-band in the same A-band (Fig. 1). Only model *e* in Fig. 6 reproduces this feature. That model *e* in Figs. 5 and 6 gives a good representation of the observed images is indicated in Fig. 7, where a micrograph and the model image are arrayed side-by-side. The obvious visual correlation is very striking. However, it should be remembered that shadowing remains an uncertain procedure and, despite the close similarity of the images in Fig. 7, the present analysis only provides one further piece of evidence about cross-bridge organization. Nevertheless support for our conclusions comes

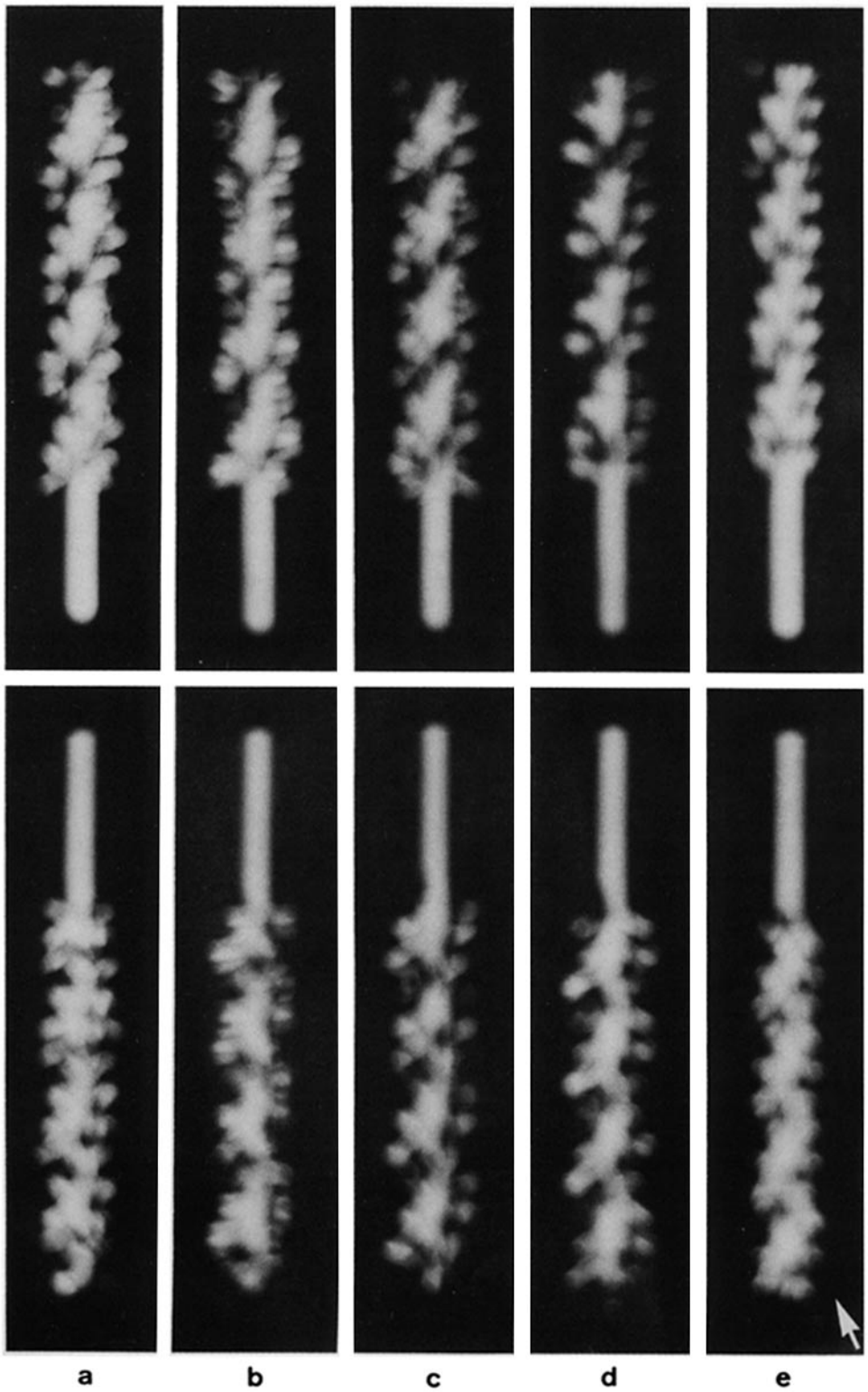

Figure 6. (*Top*) Models *a–e* in Fig. 5 but illuminated by a single point source of light at the same angle (θ = 20°) as the source of shadow in the micrographs and averages in Figs. 1, 2, and 3, and photographed with a slight defocus. (*Bottom*) Models *a–e* in Fig. 5 but this time inverted to show the effect of shadowing on cross-bridge arrays of opposite polarity, related by the dihedral symmetry of the myosin filaments across the M-band. The direction of illumination in all cases was from the lower right as indicated by the arrow. Note the marked difference in appearance in the images of filaments with opposite polarity in all cases except *e* from Fig. 5 where the differences are more subtle. For discussion see text.

from the fact that the chosen model (Fig. 5*e*) is consistent with x-ray diffraction data as described below.

Discussion

Comparison with Other Cross-bridge Arrays

Recent analysis of the cross-bridge arrays on thick filaments from muscles other than frog has either involved three-dimensional reconstruction of isolated filaments (14, 19, 29, 30) or the modelling of x-ray diffraction data (4, 6). In all cases it is clear that there is a common trend in which, however many long-pitched strands of cross-bridges there are (i.e., four for *Limulus* [29] and tarantula [14, 19]; seven for *Pecten* [30]; three for plaice and frog [4, 25, and the present work]), the myosin heads lie along these helical tracks. However, the question remains in these other cases, as in frog, whether

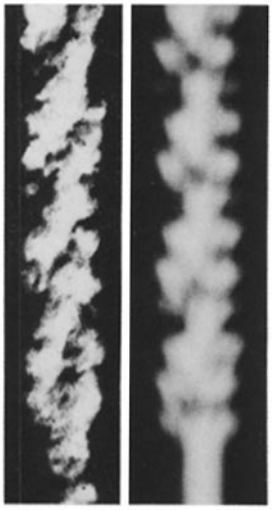

Figure 7. Comparison of (*a*) the micrograph in Fig. 2*a* after inversion with (*b*) the model in Fig. 6*e*, top. The correlation is good.

(model A) the density peaks are produced by two heads from a single myosin molecule both tilting in the same direction as in Fig. 5*e* or (model B) they are due to a single head from one myosin molecule tilting away from the bare zone and overlapping with a second head from a myosin molecule 143 Å further along the helical track and tilting back towards the bare zone (i.e., as in Fig. 5, *b* and *c*). In the case of the tarantula thick filament, the three-dimensional reconstruction by Padron et al. (19) has been interpreted in terms of the second kind of structure (B) with heads from two different myosin molecules overlapping. Work on other invertebrate muscles also seems to prefer model B (29, 30). Our present results on frog muscle thick filaments tend to favor model A, in which both heads point in the same direction, as does recent analysis of the low angle x-ray diffraction pattern from plaice fin muscle (4). It seems very likely that the similar density shapes seen on the myosin filaments in all of the invertebrate muscles mentioned so far probably mean that there is a similar, but not necessarily identical, arrangement of myosin heads in each case. However, based on present evidence for vertebrate muscle, we prefer model A in which both heads from a single myosin molecule tilt in the same direction. In this case invertebrate thick filaments are either different from those of vertebrates or their three-dimensional reconstructions have been wrongly interpreted; just as in the case of the shadowed filaments described here, interpretation of any such reconstructions is by no means a straightforward task. Thus, despite having closely related helical arrays of cross-bridge origins (22, 25), it may well be that the myosin heads in many different relaxed muscles (not insect flight muscle; 21, 26, 31) form one of two types (A and B) of head configurations on the helical arrays.

In conclusion, computer enhancement of the freeze fracture replicas obtained by Cantino and Pollack (1, 2) has produced remarkably clear images of vertebrate myosin filaments. First, these show for the first time in preparations of bulk tissue the three-stranded right-handed myosin cross-bridge helices and both of the characteristic myosin repeats of 430 Å and 140–150 Å. Second, they show that any perturbation of the cross-bridge helix of the kind proposed to account for the meridional x-ray reflections not expected from perfect helices cannot have a marked component that would move the myosin heads off the helical tracks. Analysis of the observed perturbations will be presented elsewhere. Finally, the appearance of the average images in comparison with the model structures that we have studied is consistent with a structure in which both of the heads in one myosin molecule tilt in the same direction. Of course, as mentioned earlier, such modelling does not prove that our chosen model is correct. On the other hand, by making reasonable assumptions about myosin filament structure we have been able to mimick the electron micrograph images as well as could reasonably be hoped for.

The model proposed here for the frog muscle cross-bridge array (Fig. 5*e*) is closely related to that deduced for plaice fin muscle (Fig. 5*d*) from x-ray diffraction data (4). The models are not identical, but the frog structure, with $\beta = 50–70°$, can be transposed into that for fish by a small decrease (~30°) in tilt angle. This difference in tilt is consistent with the relative weakness compared with the 429- and 215-Å layer lines of the 143-Å meridional reflection in frog muscle diffraction patterns. The intensity of the 143-Å reflection is relatively stronger in patterns from fish muscle than in frog patterns; a result that suggests that the axial tilt of the heads must be larger in frog muscle thick filaments than in fish. The smaller head tilt in fish thick filaments would also be associated with a small increase in the radius of the center of mass of the cross-bridges, an observation consistent with observed small differences between the positions of the intensity peaks on the 430-Å x-ray layer lines from the two muscles and also with the fact that the A-band lattice in fish is slightly larger in spacing at rest length than that in frog (4, 8). This agreement with other data suggests that the large tilt deduced from these shadowed replicas is a genuine feature of the cross-bridge array in vivo and is not, for example, due to a tendency of the heavy metal shadow to plaster the heads back against the thick filament shaft.

Further analysis is being carried out of images of similar preparations to those described here but shadowed in different directions. It is hoped that these preparations will contain information that will help our preference for the myosin head pairs being in conformation A rather than B and also provide evidence about whether this head tilt is towards or away from the M-band.

We are grateful for the help and support of Dr. G. Pollack in whose laboratory this project was initiated. In addition, we thank Dr. J. Koehler for the use of the Balzers BAF 301 freeze-fracture unit, and Dr. D. Johnson for the use of the JEOL 100C transmission electron microscope. We are also indebted to Dr. P. K. Luther for help with computing, to him and Drs. A. Freundlich, J. J. Harford, and H. Pask for valuable comments and for help with the generation of suitable model structures, and to Miss Gweneth Mensah for technical assistance.

This work was supported by a National Institutes of Health postdoctoral traineeship (No. HL07403) to M. E. Cantino, by a project grant from the Muscular Dystrophy Association of America to J. M. Squire, and by a program grant to J. M. Squire from the British Medical Research Council.

Received for publication 3 June 1985, and in revised form 4 October 1985.

References

1. Cantino, M. E., and G. H. Pollack. 1983. Cross-bridges in relaxed and activated skinned muscle fibers. *Biophys. J.* 41:264a. (Abstr.)
2. Cantino, M. E., and G. H. Pollack. 1984. Propane-jet freezing of muscle

fibers for freeze fracture. *Proc. 42nd E.M.S.A. Meeting.* G. W. Bailey, editor. San Francisco Press Inc., San Francisco. 10–11.

3. DeRosier, D. J., and P. B. Moore. 1970. Reconstruction of three-dimensional images from electron micrographs of structures with helical symmetry. *J. Mol. Biol.* 52:355–369.

4. Harford, J. J. 1984. Diffraction analysis of vertebrate muscle crossbridge arrangements. Ph.D. Thesis. London University.

5. Haselgrove, J. C. 1975. X-ray evidence for conformational changes in the myosin filaments of vertebrate striated muscle. *J. Mol. Biol.* 92:113–143.

6. Haselgrove, J. C. 1980. A model of myosin crossbridge structure consistent with the low angle X-ray diffraction pattern of vertebrate muscle. *J. Musc. Res. Cell Motil.* 1:177–191.

7. Heuser, J. 1981. Quick-freeze, deep-etch preparation of samples for 3-D electron microscopy. *Trends Biochem. Sci.* 6:64–68.

8. Huxley, H. E., and W. Brown. 1967. The low-angle X-ray diagram of vertebrate striated muscle and its behavior during contraction and rigor. *J. Mol. Biol.* 30:383–434.

9. Huxley, H. E., R. M. Simmons, A. R. Faruqi, M. Kress, J. Bordas, and M. H. J. Koch. 1981. Millisecond time-resolved changes in X-ray reflections from contracting muscle during rapid mechanical transients, recorded using synchrotron radiation. *Proc. Natl. Acad. Sci. USA.* 78:2297–2301.

10. Huxley, H. E., A. R. Faruqi, M. Kress, J. Bordas, and M. H. J. Koch. 1982. Time-resolved X-ray diffraction studies of the myosin layer-line reflections during muscle contraction. *J. Mol. Biol.* 158:637–684.

11. Ip, W., and J. Heuser. 1982. Myosin cross-bridge structure and attachment to thin filaments viewed by a new approach. *J. Cell Biol.* 95(2, Pt. 2):367a. (Abstr.)

12. Ip, W., and J. Heuser. 1983. Direct visualisation of the myosin cross-bridge helices on relaxed rabbit psoas thick filaments. *J. Mol. Biol.* 171:105–109.

13. Kensler, R. W., and M. Stewart. 1983. Frog skeletal muscle thick filaments are three stranded. *J. Cell Biol.* 96:1797–1802.

14. Levine, R. J. C., R. W. Kensler, M. C. Reedy, W. Hofmann, and H. A. King. 1983. Structure and paramyosin content of tarantula thick filaments. *J. Cell Biol.* 97:186–195.

15. Luther, P. K., and J. M. Squire. 1978. Three-dimensional structure of the vertebrate muscle M-region. *J. Mol. Biol.* 125:313–324.

16. Luther, P. K., P. M. G. Munro, and J. M. Squire. 1981. Three-dimensional structure of the vertebrate muscle A-band III, M-region structure and myosin filament symmetry. *J. Mol. Biol.* 151:703–730.

17. Muller, M., N. Meister, and H. Moor. 1980. Freezing in a propane jet and its application in freeze fracturing. *Mikroskopie.* 36:129–140.

18. Offer, G., J. Couch, E. J. O'Brien, and A. Elliott. 1981. Arrangement of cross-bridges in insect flight muscle in rigor. *J. Mol. Biol.* 151:663–702.

19. Padron, R., R. A. Crowther, and R. Craig. 1984. The spatial arrangement of both heads of the myosin molecule on relaxed tarantula muscle thick filaments. *IUPAB 8th Intl. Biophys. Congr., Bristol.* 010:P. 199. (Abstr.)

20. Poulsen, F. R., and J. Lowy. 1984. Application of potential energy calculations to the determination of muscle structure from X-ray data with special reference to the configuration of myosin heads. *J. Mol. Biol.* 174:239–247.

21. Reedy, M. K., and W. E. Garrett, Jr. 1977. Electron microscope studies of *Lethocerus* flight muscle in rigor. *In* Insect Flight Muscle. R. T. Tregear, editor.) Elsevier North-Holland, Amsterdam. 15–135.

22. Squire, J. M. 1971. General model for the structure of all myosin-containing filaments. *Nature (Lond.).* 233:457–462.

23. Squire, J. M. 1972. General model of myosin filament structure II. Myosin filaments and crossbridge interactions in vertebrate striated and insect flight muscles. *J. Mol. Biol.* 72:125–138.

24. Squire, J. M. 1981. The Structural Basis of Muscular Contraction. Plenum Publishing Corp., New York. 698 pp.

25. Squire, J. M. 1985. Muscle myosin filaments: internal structure and crossbridge organisation. *In* Comments on Molecular and Cellular Biophysics. Gordon and Breach, New York. In press.

26. Squire, J. M., A-C. Edman, A. Freundlich, J. J. Harford, and M. Sjostrom. 1981. Muscle structure, cryo-methods and image analysis. *J. Microsc.* 125:215–225.

27. Squire, J. M., J. J. Harford, A-C. Edman, and M. Sjostrom. 1982. Fine structure of the A-band in cryo-sections. *J. Mol. Biol.* 155:467–494.

28. Starr, R., and G. Offer. 1983. H-protein and X-protein. Two new components of the thick filaments of vertebrate skeletal muscle. *J. Mol. Biol.* 170:675–698.

29. Stewart, M., R. W.. Kensler, and R. J. C. Levine. 1981. Structure of *Limulus* Telson muscle thick filaments. *J. Mol. Biol.* 153:781–790.

30. Vibert, P., and R. Craig. 1983. Electron microscopy and image analysis of myosin filaments from scallop striated muscle. *J. Mol. Biol.* 165:303–320.

31. Wray, J. S. 1979. Filament geometry and the activation of insect flight muscles. *Nature (Lond.).* 280:325–326.

32. Yagi, N., E. J. O'Brien, and I. Matsubara. 1981. Changes of thick filament structure during contraction of frog striated muscle. *Biophys. J.* 33:121–138.